Final Technical Report (UMD AMAV)

1. Executive Summary

1.1. Objective Statement

Under the VFS Design-Build-Vertical Flight Competition guidelines, the University of Maryland Autonomous Micro Air Vehicle (AMAV) team's overall objective is to develop and fabricate an unmanned aerial vehicle capable of completing a flight performance and an autonomy course. The UMD AMAV's Tailsitter design named *Foxtail* is shown to the right.

UMD AMAV Foxtail

1.2. Purpose of Design

The design of the vehicle seeks to be as maneuverable and efficient as possible, include autonomous flight capabilities, and remain under strict competition guidelines such as weight limit, payload requirement, dimensions, and overall design quality. Safety, reliability, ease of manufacturing, material sustainability, component and flight testing processes also inform and validate the overall design process.

1.3. Planned Approach

The UMD AMAV team's plan for the VFS DBVF Competition involved a multistep process to create a successful and innovative design. We began with a detailed schedule that was consistently updated as necessary with every step of our design, manufacturing, and testing processes (Section 2). At the start of the design process, we began by outlining the mission requirements to create our own design plan (Section 3.1). We narrowed down the major priorities for our design based on the competition scoring criteria, budget constraints, and manufacturing feasibility (Section 3.2). From the breakdown of the main design priorities, we developed a number of configurations to determine the best fit for this competition (Section 3.3). After populating a decision matrix, we selected our final design configuration to be a tailsitter configuration and performed further down selection for the number of rotor blades and wing-rotor arrangement (Section 3.4). While the overall goal of the design is to be successful in the competition, we emphasized uniqueness and incorporated the latest manufacturing technologies to support safety and sustainability goals (Section 4). To move forward from this preliminary design to the final design (Section 5), 3D drawings were developed that allow traceability of the design process as well as a simpler replication in the event of successful design (Section 6). Our manufacturing process included facilities and resources available at the

University of Maryland, as well as vendors providing specialized services (Section 7). At the termination of the final design stage, we tested every component and sub-components of our vehicle to ensure its reliability and identify any possible failure modes so that the appropriate adjustments to the vehicle could be made (Section 8 and 9). The completed tests validate the overall performance of the vehicle developed for the competition. Additional tests and full mock mission tests will continue up until the final presentation (Section 9) and flight exhibition, as appropriate.

2. Management Summary

2.1. Team Organization

The AMAV team is composed of undergraduate and graduate students from aerospace engineering, computer science, and robotics. The team is guided by advisor, Prof. Derek A. Paley, Director of the Maryland Robotics Center. The overall team lead is Animesh Shastry and co-lead is Wei Cui, both Ph.D. students in the Aerospace Engineering department. The team's primary pilot is Qingwen Wei and backup pilot is Dogyu Jun, both undergraduate students in Aerospace Engineering. The AMAV team is organized into the following three working groups: vehicle CAD is performed by Dhruv Srinivasan, an undergraduate in Mechanical Engineering; vehicle flight performance analysis is performed by John Soong, a master student in Aerospace Engineering; manufacturing and flight testing is performed by all the team members. In addition to the above people, includes robotics graduate students Adarsh Malapaka and Sagar Vijayakumar, along with aerospace undergraduate students Dogyu Jun and Thomas Brosh.

2.2. Schedule

A Gantt chart showing the complete build and flight test timeline is provided below. We are not aware of any remaining long-lead or high-risk items in our build plan. However, the autonomous landing accuracy and full-length mock mission testing poses a mild to moderate risk of crash.

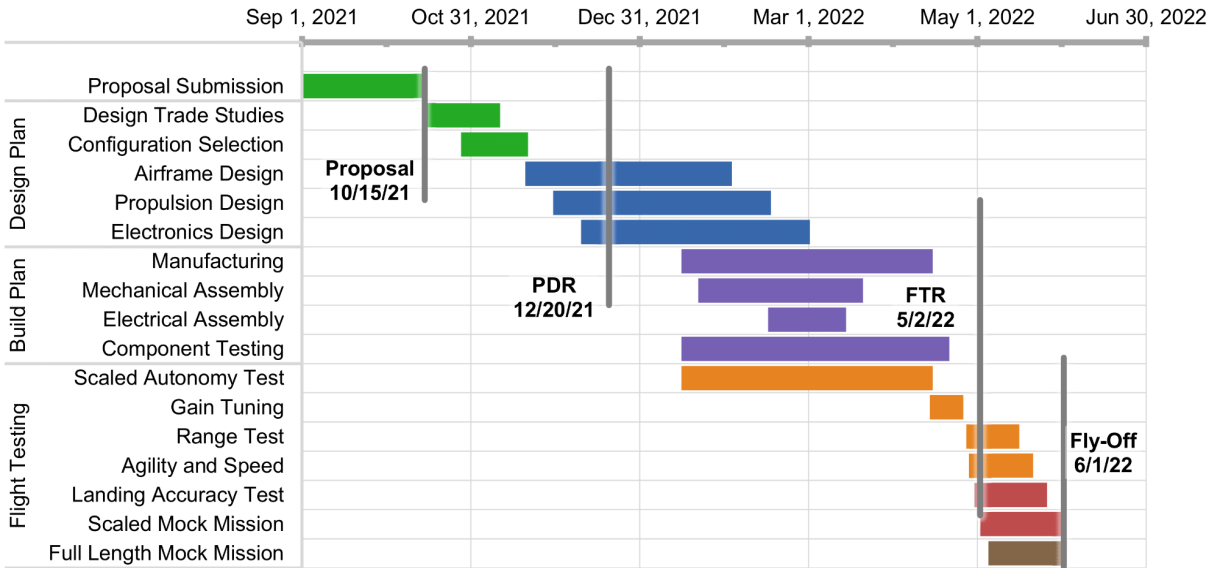

3. Design Trade Studies

3.1. Mission Requirements

The vehicle must be able to successfully complete the following two courses to earn points dictated by the rubric on the Request for Proposal (RFP).

Flight Performance Course: This course tests the vehicle's agility and endurance by having the vehicle complete as many laps of a predetermined course as it can in under ten minutes. Before takeoff, a 2-lb SoftGrip weight is attached to the vehicle with an option for heavier weights if needed. The vehicle must perform a full VTOL landing and take-off within each landing zone. Finally, the vehicle must land within the start/end VTOL zone before time expiration to avoid a 3-lap deduction penalty. The course is scored on three parameters: lap time, number of laps completed, and payload weight, each of which is scored out of 50 points.

Autonomy Course: The vehicle must maneuver autonomously through the course using pre-set GPS coordinates. The waypoints also follow the same waypoints as the previously mentioned course. A successful completion of the course yields 150 points.

3.2. Design Drivers

Endurance and Maneuverability: For the competition, our primary goal is to fly as fast as possible to maximize the number of laps within the allotted 10 minutes flight time. Approximately 66% of the overall fly-off points comes from the endurance and maneuverability of the design. Hence, we sought a design with a greater motor thrust or a design with a higher number of motors to increase our ability to accelerate quickly and minimize turning radius.

Weight/Dimensions: For the aircraft design, one of our goals was to make the best use of the provided hard dimensional constraints, i.e., a 6.5ft maximum span and a maximum weight of 15-lb including the 2-lb payload. Since 33% of the overall points come from our payload fraction, part of our team's design process involved leaving ample room for additional payload weight.

Cost and Reliability: Although we have benefited this year and in prior years from generous support of our sponsors including the Maryland Robotics Center and Leidos, the cost of components and manufacturing was factored into our overall decision process. In areas where we could lean for a lower-cost alternative, we attempted to do so. However, for the propulsive system components of our drone, we valued reliability more than cost.

Design Complexity: It is important that the proposed aircraft design is not overly complex, since it may impact manufacturing time, cost, and reliability. Further, unnecessary complexity may have a negative impact on controllability. During the design process, we valued configurations that were not overly complex, which could have hampered manufacturing or ease of piloting.

3.3. Configurations Considered

The configurations considered focused on maximizing speed and efficiency between waypoints. The nature of the mission's timed component led the team to favor configurations with a fast cruise speed; however, the ability to transition between hover and forward flight was an

important caveat to this consideration. The team also focused on designs in which autonomous navigation, including forward-flight and hover transition control actions, were relatively easy to implement. The following configurations were considered:

Configuration	Description
	**Quadrotor** - Most common drone configuration with four rotors - Control angles determined by varying RPM of motor(s) - Forward flight achieved by pitching vehicle forward - Motor used: KDE6213XF-205 | Prop size: 24.5 x 8.1 (Dual-bladed)
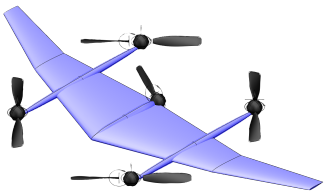	**Quadplane** - Configuration has four rotors with fixed wing/aircraft fuselage - Forward flight conducted by pusher propeller - Pitch, roll determined by varying rotor RPM or aircraft control surfaces - Rotor motor used: KDE6213XF-185 | Prop size: 24.5 x 8.1 (Dual-bladed) - Pusher motor used: KDE600XF-1100-G3 | Prop size: 10x8 (Dual-bladed)
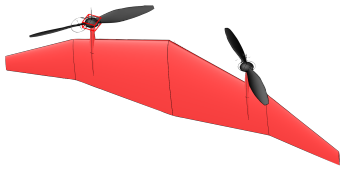	**Tailsitter** - Configuration that starts vertically then tilts the entire fuselage forward to transition into forward flight. - Transition achieved by pitching vehicle forward - Motor used: KDE6213XF-185 | Prop size: 24.5 x 8.1 (Dual-bladed)
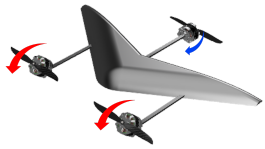	**Tiltrotor** - Configuration with either two or three tilting rotors - Control angles determined by tilting rotors - Forward flight achieved by tilting rotor along vehicle's longitudinal axis - Motor used: KDE6213XF-205 | Prop size: 24.5 x 8.1 (Triple-bladed)

3.4. Selection Process and Final Design

3.4.1. Analysis of Alternative Configurations

Before selection, an internal review of the configuration was conducted among the team for configuration finalization. Factor weightings and ultimate decisions were cataloged in a decision matrix. The quadplane and tiltrotor configuration have some similarities that may overlap in design, so the quadplane model is assumed to be a four-rotor model with a pusher/tractor propeller, whereas the tiltrotor is a tricopter configuration. We used the Analytical Hierarchy Process (AHP) method to obtain weights for each of the parameters. The resulting Pugh Matrix is given in Table 1.

The two key parameters that influenced the team's decision were safety and reliability, followed by maneuverability and endurance. A high thrust-to-weight ratio provides greater maneuverability of the vehicle. In the case of both the tailsitter and tiltrotor, the aforementioned parameter also allows the vehicle to achieve cruise speed faster. Payload fraction is also an important parameter. A lower frame weight allows for a higher payload capacity. In addition to the aforementioned parameters, the team also considered cost and design complexity. While there is no restriction on the amount spent, the team valued designs whose parts could be

manufactured in-house through methods such as additive printing. Design complexity embodied both ease of assembly, disassembly, and pilot control.

Table 1. Pugh Matrix for Configuration Selection. The various configurations are compared against the quadrotor baseline and are scored from +3 to -3 denoting the degree of fulfillment of each design goal.

Design Driver	Score Weight	Quadrotor	Quadplane	Tailsitter	Tiltrotor
Endurance	*1.4*	0	+3	+3	+2
Maneuverability	*1.5*	0	-2	-1	-2
Payload Fraction	*0.5*	0	-2	-1	-2
Cost	*0.2*	0	-1	-1	-2
Reliability	*1.7*	0	+1	+1	+1
Design Complexity	*0.3*	0	-2	-2	-3
Forward Flight Performance	*0.5*	0	+3	+2	+2
Safety	*2.2*	0	0	0	-1
Final Score		**0.0**	**2.4**	**4.0**	**-2.3**

3.4.2. Selection and Customization of Final Design

Based on the decision matrix, the team selected the tailsitter configuration for this year's design. The timed nature of the flight performance course strongly incentivizes a fast cruise speed between waypoints with fewer actuators such as motors or servos. The quadplane, tiltrotor, and tailsitter all perform well in this category, but the tailsitter has the least weight; this design maximizes the payload fraction. The tailsitter design has similar performance characteristics to that of the standard quadcopter in hover and low speed flight, which simplifies implementation of autonomous navigation and accurate landing.

Wing and rotor arrangement: In the class of tailsitter vehicles, several arrangements of wing and rotors are possible based on desired flight characteristics. The team brainstormed and qualitatively compared the following possible wing-rotor arrangement for tailsitter vehicle type. The blue circles represent the rotors and the red lines represent the wing(s) as viewed from top.

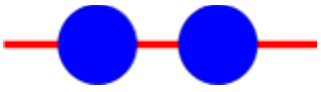

1. Monoplane Dualrotor

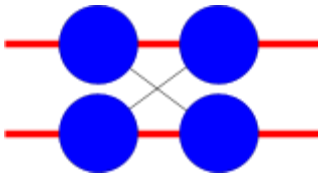

2. Biplane Quadrotor type 1

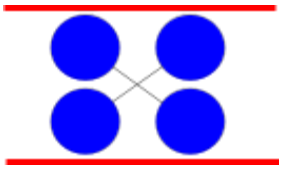

3. Biplane Quadrotor type 2

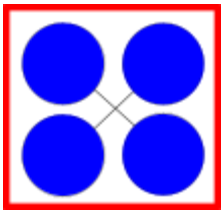

4. Boxed Wing Quadrotor

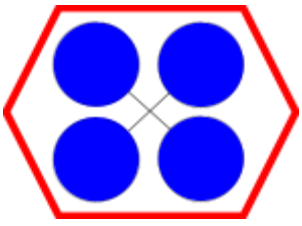

5. Hexagon Wing Quadrotor

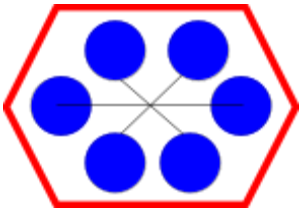

6. Hexagon Wing Hexarotor

We rejected arrangement 1 above because, to create a pitching moment, control surfaces would have to be added, which would lead to lower control authority in hover and transition. We rejected arrangement 6 because it has the lowest rotor size among all the arrangements and hence has reduced hover efficiency due to higher disk-loading. We rejected arrangement 4 because it has the lowest wing area for generating lift, though the large side wings would lead to the best cornering performance in flight. Hence, given the 6.5 ft vehicle size constraint, the arrangement that leads to the largest rotor and effective lifting wing area are arrangements 2, 3, and 5. Arrangements 2 and 3 would lead to more efficient cruise compared to 5, but the lack of side wings would impact cornering performance, i.e., the vehicle nose would have to point towards the center of turn. Additionally, the shroud structure of arrangement 5 would provide safety to ground personnel. Hence, we selected the *Hexagon Wing Quadrotor Tailsitter* configuration.

Rotor blade downselection: The two efficiency metrics used for rotor selection are the *Thrust-to-Power ratio* (also known as Power Loading) and the *Figure of Merit* (FoM). Thrust-to-Power is the primary efficiency metric for selecting any motor propeller combination. It is affected by a number of factors ranging from motor-kv, ESC performance, electrical power losses and rotor blade's aerodynamic efficiency. The FoM on the contrary is defined as the ratio of ideal hover power to total hover power and it represents how close a particular rotor is to the ideal rotor. A simplified FoM expression is provided below:

$$FoM = \frac{Ideal\ Hover\ Power}{Total\ Hover\ Power} = \frac{Ideal\ hover\ power}{Induced\ Power + Profile\ Power}$$

A higher FoM leads to better Power loading and thus more efficient rotor performance. FoM can be increased by reducing induced power or profile power. The induced power is independent of the number of rotor blades and hence, the profile power can be lowered to increase FoM. Hence, a 2-bladed rotor will have better FoM than rotors with 3 or higher number of blades. Additionally, even though FoM is not defined for cruise, having a lower profile power will lead to more efficient cruise. Therefore, we selected a 2-bladed rotor configuration for our design.

4. Technical Innovations

4.1. Safety and Sustainability

Shrouded Angled wings: To increase agility, we reduced the tailsitter's transition time between hover and cruise flight. Angling the wings by 30° from the vertical as shown in Figure 1, the aircraft needs to pitch only 60° to enter cruise mode. Additionally, since safety is an important factor in our design, the wing shroud provides an appropriate level of safety and ensures that ground personnel are not directly exposed to spinning rotor blades.

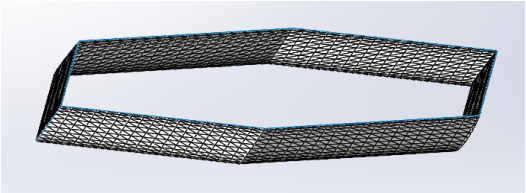

Fig. 1. Shrouded Angled Wings Concept

Electronics Protection: In addition to the required shunt-plug and fuse, the electronics and PCBs on the aircraft are protected from dust, light rain, and adverse environmental conditions by application

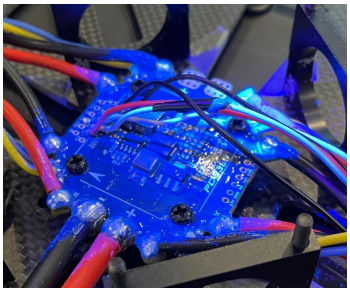

Fig. 2. Conformal coating shown under UV light

of acrylic conformal coating. The acrylic resin is applied to the Power Distribution Board (PDB) as shown in Figure 2 and the Electronic Speed Controllers (ESCs).

3D Printing: Due to the fast-paced nature of the competition timeline, we are taking the advantage of 3D printing technology. We can choose between different types of plastic, polymer, and carbon-based filaments to create customized parts. The low cost of 3D printed parts also allows for easy testing of parts that need to be CNC machined. Additionally, 3D printing leads to less material waste compared to the traditional subtractive machining processes. Furthermore, components that are not a part of the aircraft but were utilized during the assembly process were 3D printed from recycled, chopped filaments, which reduced plastic waste and helped us in achieving higher sustainability goals.

Aircraft design benefits from components that are lightweight and durable, with the ability to sustain loads in all directions due to the drone rapidly transitioning between vertical and forward flight. With these factors in mind, we opted to use Onyx, a nylon based filament, for stiff structural components such as the arm-wing connectors. The material's high heat deflection temperature allows us to reinforce the material with carbon fiber inlay to significantly increase its already large baseline tensile strength of 36MPa. With 20% carbon fiber inlay tensile strength increases to 192MPa. For the carbon fiber inlay, we opted to use an Isotropic Fiber fill to withstand loads from all directions, ensuring that our components can withstand the drone transitioning between vertical and horizontal flight. Additionally, we chose flexible components to reduce landing impacts. We experimented with digital materials capable of producing a wide range of flexible components based on the proportion of two or more resins. By mixing Agilus30 black and vero white resins different shore hardness and tensile strengths can be achieved. Table 2 shows the different material types that can be 3D printed by adjusting the proportion.

Table 2. Properties of Digital Materials created by mixing Agilus30 black with Vero white

Property	**Unit**	**FLX9840**	**FLX9870**	**FLX9885**	**FLX9895**
Tensile Strength	MPa	3-4	4-6	6-10	10-14
Elongation at break	%	190-210	120-140	70-90	50-70
Shore Hardness	Scale A	40-50	60-70	80-85	85-90

FLX9840 is pure Agilus30 black and its lower hardness will lead to the largest impact absorption from converting mechanical energy to heat, i.e., hysteresis. Hence, it is used for the landing gear feet as it is not a structural component but needs to have the highest impact absorption. On the contrary, for the landing gear to arm mount more strength and stiffness is desired with flexibility and hence we used FLX9895 for it. Further discussion of this is presented in *Section 6.3*.

Expanded Polypropylene (EPP) Foam Cut: The whole wing was fabricated using EPP Foam, which has good impact, water, and chemical resistance. It is a widely used material in fabricating RC planes. A hot-wire cutting method was used to make the wings; this method ensured a clean surface and low cost. The wings are laminated using a standard film, to provide debris resistance and added integrity during forward flight.

4.2. Mission Model

Assumptions and Uncertainties: Standard rotorcraft flight assumptions include 20% efficiency loss, flight at ISA+15℃ conditions with air density ρ = 0.002377 slug/ft³, and canceling of rotor in-plane forces and moments due to the symmetry of rotor placement. For the purposes of calculation, the rotor blade is assumed to be rectangular, untwisted, and rigid with an 8:1 radius-to-chord ratio based on the manufacturer's design. Assume uniform inflow across the rotor. Uncertainties include the final frame weight of the vehicle itself.

Sources of Inputs: The other main input into the mission power estimation model is the aerodynamic force model. The aerodynamic lift and drag are obtained from XFLR5 analysis of the wings; see Section 4.3. Motor thrust and RPM are calculated using the aerodynamic force model in the trim procedure.

Detailed Model Description: Power estimation for the vehicle in hover was performed using the helicopter trim procedure detailed in Algorithm 1 from helicopter aerodynamics [1]. A power-velocity diagram was used to estimate the vehicle's endurance and range using approximations for fuselage and wing drag. Algorithm 2 summarizes the vehicle power calculation procedure in forward flight [2].

Algorithm 1 Vehicle Power calculation in hover

1: Initialize vehicle model parameters $W, \Omega, \rho, A, R, \sigma$
2: Thrust: $T \Leftarrow W$
3: Thrust coefficient: $c_T \Leftarrow \frac{T}{\rho A(\Omega R)^2}$
4: Induced power coef.: $c_{P_i} \Leftarrow \sqrt{\frac{c_T}{2}}$
5: Profile power coef.: $c_{P_o} \Leftarrow \frac{\sigma c_{d_0}}{8}$
6: Total Power: $P \Leftarrow \rho A(\Omega R)^3(c_{P_i} + c_{P_o})$

Result: P

Algorithm 2 Vehicle power calculation in forward flight

1: Initialize vehicle model parameters $W_{lb}, \rho, b_{wing}, c_{wing}$
2: Initialize c_{d_0} from NACA 2412
3: Oswald efficiency: $e \Leftarrow 0.8$
4: Weight in metric: $W_N \Leftarrow 4.45 W_{lb}$
5: Flat-plate estimation: $f \Leftarrow 1.5(\frac{W_{lb}}{1000})^{0.7263}$
6: Airspeed: $u \Leftarrow [5:50]$ m/s
7: Wing area: $S \Leftarrow \frac{b_{wing}}{c_{wing}}$
8: Dynamic pressure: $q \Leftarrow \frac{1}{2}\rho U^2$
9: Lift coefficient: $c_l \Leftarrow \frac{W_N}{qS}$
10: Wing drag coefficient: $c_d \Leftarrow c_{d_0} + \frac{c_l^2}{\pi e \frac{b}{c}}$
11: Wing drag: $D_{wing} \Leftarrow qSc_d$
12: Fuselage drag: $D_{fuselage} \Leftarrow qf$
13: Total drag: $D \Leftarrow 2D_{wing} + D_{fuselage}$
14: Required power: $P \Leftarrow 1.341 \frac{du}{1000}$ in HP

Result: Plot P vs. u

4.3. Aircraft Transition Process

Due to the angled wings of the aircraft, the required pitch angle in cruise is around 60°. Figure 2 shows the aircraft transitioning from hover to cruise mode and then returning to hover mode. The two widely-used open-source firmwares, PX4 and ArduPilot, both contain the tailsitter configuration. However, we will modify the cruise attitude parameter to reflect proper control mixing for our vehicle design. Figure 3 shows a typical flight scenario where the aircraft takes off, hovers and performs transition to cruise. When the cruising aircraft reaches its destination, it transitions back to hover and lands.

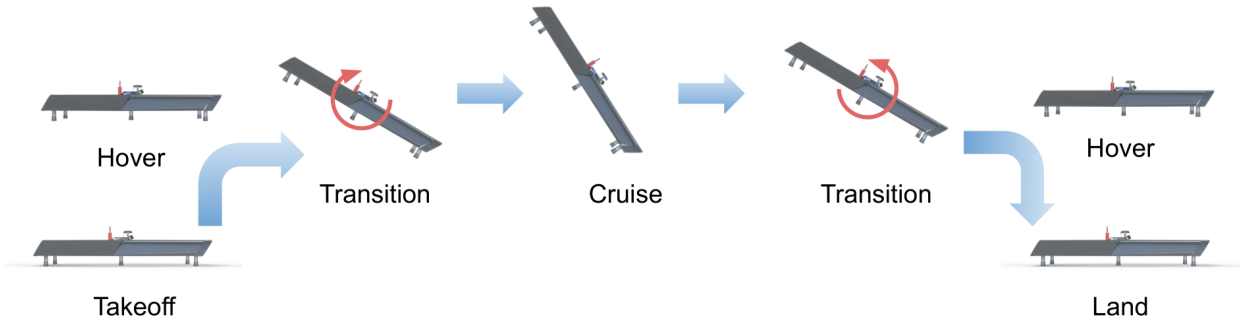

Fig. 3. The maneuvers performed by the aircraft in a standard mission

5. Design Definition

5.1. Overall vehicle design

The vehicle shown in Figure 4 is a hybrid VTOL aircraft consisting of four motors organized in a quad configuration. To increase cruise performance, it has a biplane wing structure with fins that connect to form a hexagonal wing shroud. The vehicle, though technically in the class of tailsitter aircraft, has wings that are angled in such a way that the aircraft has to pitch by only 60° to transition between hover and cruise, which reduces transition height and time. The wings also shroud the propellers to provide safety for ground personnel.

5.2. Vehicle sub-system design

Fig. 4. Overall Vehicle Design

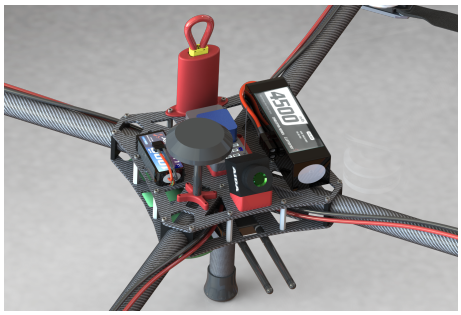

Fig 5. Central Frame

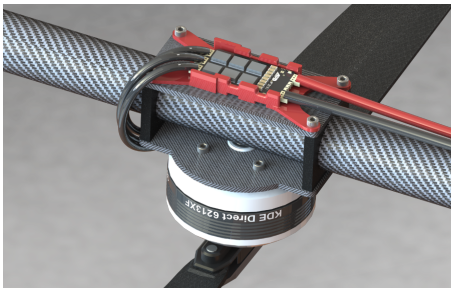

Fig. 6. Motor Mount

5.2.1. Airframe

The central frame of the aircraft shown in Figure 5 holds the electronics and batteries. It is a 8.5”x8.5” carbon fiber plate of 0.12” thickness. The plates have a twill weave finish and a quasi-isotropic layup. It also supports the 7” shunt plug tower with incorporated 100A fuse for

the main flight battery to meet the competition requirements. The four arms of the aircraft manufactured by DragonPlate are axially optimized carbon fiber tubes of 2.6 ft in length and 1.12” outer diameter. The motors on the aircraft are pusher type, which leads to better agility and endurance and, in cruise, moves the center of gravity forward in the body frame. The motor mounts as shown in Figure 6 are made from anodized aluminium and use a compression mounting technique to preserve the structural integrity of the arms. 3D printed connectors made from onyx at the ends of each arm connect them to the wing spars, which are pultruded carbon fiber tubes of 0.5” outer diameter. A NACA2412 airfoil is used for the main top and bottom wings, and NACA0012 for the fins. The wings have a chord of 5.9” and are made up of #1.3 EPP foam. The total weight of the aircraft is estimated to be 12 lbs with a payload capacity of 3 lbs.

5.2.2. Propulsion System

Motors: Five motors of varying sizes and kV ratings from KDE Direct were considered for this year’s design. The primary efficiency metric for motor selection is the thrust-to-power ratio. For a constant source voltage the efficiency metric becomes thrust-to-current ratio. A secondary factor for motor selection is the maximum amount of thrust that a motor can generate which should result in a max thrust-to weight ratio of at least 3. Essentially, there must be sufficient control bandwidth to achieve agile flight characteristics. Figure 7 shows the current vs. thrust for the motors, all configured with a 24.5x8.1 dual-bladed propeller. The best motor for maximum thrust-to-current ratio is the KDE7215XF-135, the lowest kV motor. However, it has the lowest maximum thrust among all and using this will result in poor agility. The KDE6815XF-205 motor can produce the most amount of thrust but it is not as efficient as KDE7215XF-135. The KDE6213XF-185 motor’s thrust-to-current ratio is in between the above two and thus was ultimately chosen since it is also 0.47-lb lighter than the KDE6815XF-205 while still producing considerable thrust at a more efficient rate. The estimated maximum thrust-to-weight ratio is 3.4 when the aircraft’s weight is 15lbs, a pessimistic scenario. Thus, this motor balances efficiency and maneuverability to yield an optimal configuration.

Rotor/Propeller: The two driving metrics for selecting propellers are Disk Loading (DL) and Figure of Merit (FoM). Airfoil shape would have also been a factor, but this data cannot be obtained from the manufacturer. The blade pitch is another factor for selection, but its value is tightly related to the diameter and is completely under the control of the manufacturer. Hence, as explained in Section 3.4.2 we selected a two-bladed rotor type to decrease profile power and thereby increase the FoM. Additionally, a 24.5” propeller is the largest that can fit within the wing structure with appropriate clearance; larger propellers lead to lower disk loading and more efficient flight. Therefore, we selected 24.5x8.1 dual-bladed propellers from KDE.

Batteries: The battery choice was based on the chosen motor and propeller combination’s current demand in hover and the ability to power the motors for more than 10 min. One Lumenier 4500mAh 6S 120c battery will give around 12 min of hover. In cruise, the additional lift from the wings will support the vehicle weight and thus the flight time is expected to stay the

same. The avionics and FPV gear will be powered from a separate 1000mah 3S battery, which will allow stable supply of power and hotswaps of the flight batteries without needing to power down the avionics.

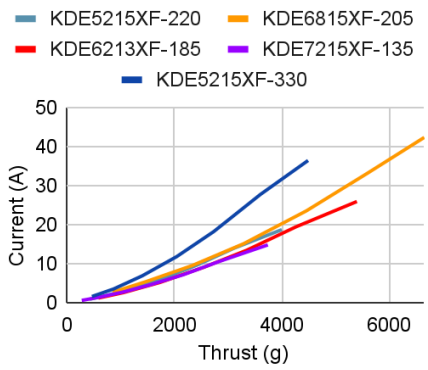

Fig. 7. Motor Thrust Data from Manufacturer (KDE Direct)

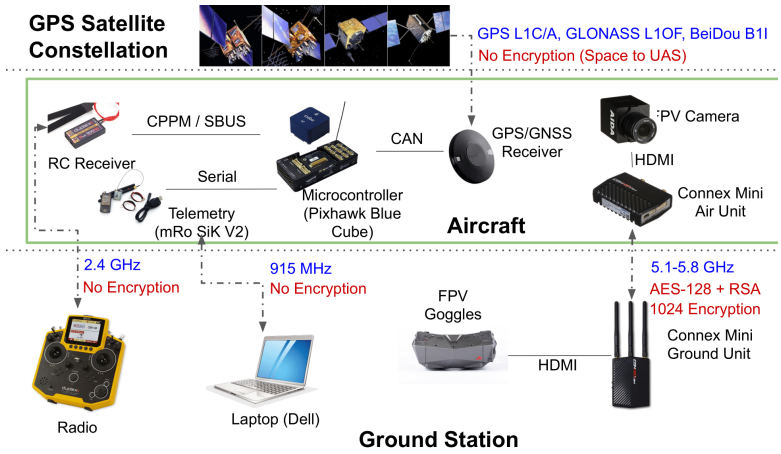

Fig. 8. Aircraft Autonomy Network

5.2.3. Electronics

Pixhawk 2.1 Blue Cube and Here3 GPS: The Pixhawk 2.1 Blue Cube was chosen for its reliability and autonomous capabilities. It features a triple-redundant IMU that is temperature controlled and shock-resistant. This allows for additional safety as the IMU is the primary sensor needed for manual flight, allowing the possibility of maintaining control of the aircraft in manual mode should other sensors fail. Our Pixhawk is paired with a single Here3 GPS.

Connex Mini Wireless HD Video Link: This system transmits live video footage on the 5.1-5.8 GHz band. It supports 1080p 60fps video transmission with less than 1ms latency, allowing for safe operation of the aircraft. It has a LoS range of 1600ft and AES+RSA encryption.

Advanced Power Drives Electronic Speed Controller: These ESCs were originally intended for X-class racing drones and feature an F3 processor that accepts DShot input commands, which create a reliable and low-latency connection between the ESC and flight controller. We selected the 80F3[X] series ESC, which supports 8S and 80A, since the higher rating of the ESC leads to cooler and more reliable operations.

5.2.4. Autonomous Flight

We use QGroundControl as our ground control station (GCS) software to configure autonomous waypoint missions. A connection with the aircraft and the ground station (Figure 8) is established with the help of MAVLink via telemetry radio. The waypoints for each mission are set using QGroundControl. The mission file is uploaded to the Pixhawk through MAVLink via radio telemetry.

5.3. Aircraft Structural Analysis

The objective of this analysis is to make sure that the carbon fiber composite components of the aircraft survive at 9g flight condition with a high Factor of Safety margin (>10) so that in the event of non severe crashes the aircraft maintains its structural integrity. Furthermore, we assume

the Ultimate Tensile Strength of carbon-fiber composites as 3.5 GPa which is less than the manufacturer's specification of 4.4 GPa in order to account for uncertainty due to structure damage or normal wear and tear.

Central Frame: To analyze the central frame in isolation, the forces considered are concentrated to where the arms connect to the frame via the frame mounts. At 9g acceleration, each of the arm mounting points experience 132.3 N, distributed over the mounting surface. It represents a worst case stress indicative of loads experienced during fast acceleration. The places where the upper frame is mounted to the lower frame were fixed during simulation. As shown in Figure 9, a maximum stress of 293 MPa is reported, which results in a Factor of Safety of 11.8 at 9g acceleration condition. In conclusion, the frame's high safety margin ensures that it will not exceed its safety bounds during flight and will maintain its structural integrity in non severe crashes.

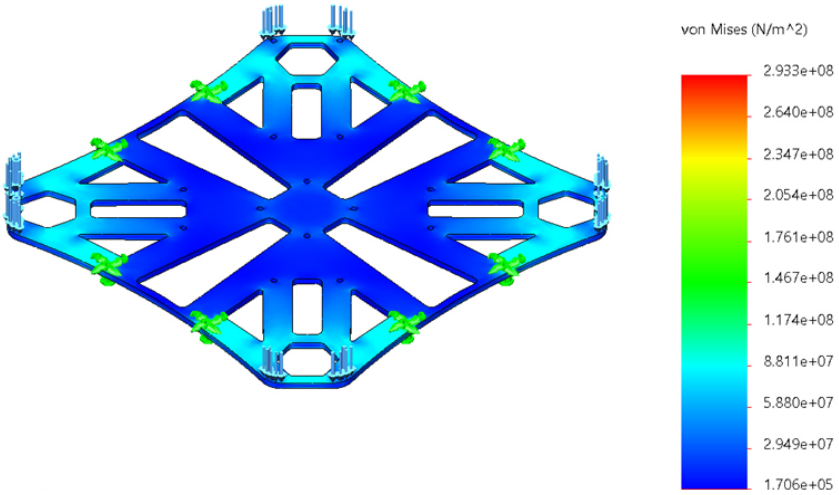

Fig. 9. Stress plot of the bottom central frame plate

Arms: A similar loading scenario at 9g acceleration was tested on the arms. Forces are applied where the arms are mounted to the motors. The maximum stress reported is 101.9 MPa (Figure 10), which results in a Factor of Safety of 34.3—around 3 times more than the central frame.

Spars: The spars of the main wings were subject to an upward directed distributed load of 15.3 kgf, which assumes that the top and bottom wing support half the vehicle weight in cruise and 9g acceleration flight. The maximum stress reported was 133 MPa (Figure 11), which results in a Factor of Safety of 26.3—around twice that of the central frame.

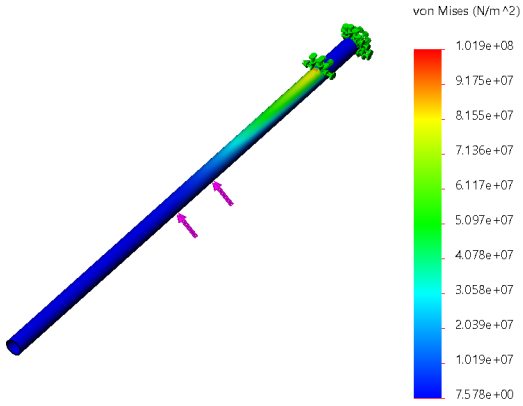

Fig. 10. Stress plot on the arm

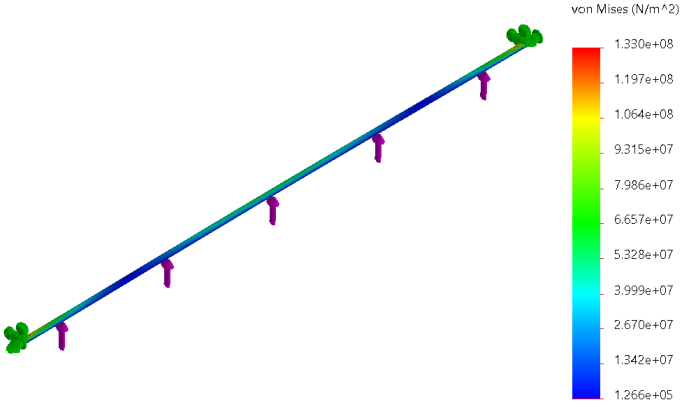

Fig. 11. Stress plot on a wing spar

5.4. Aircraft Performance Analysis

Predicted Mission Performance: The power calculations were performed at the maximum allowable competition weight of 15 lbs. Most rotorcraft consume the most power while in hover, so calculating the hover endurance yields an upper threshold. At the maximum weight, each motor must output about 3.75 lbs of thrust. As a result, each motor draws 5.1 A of current or 20.4 A in total. Assuming a depth of discharge of 80%, the vehicle has an endurance of 10.6 minutes in hover. Figure 12 shows the power-velocity diagram that was generated to find range and endurance estimates in forward flight. Speed for best endurance occurs at the minimum of the power-velocity curve, which is 41.75 ft/s with a corresponding minimum required power of 0.5667 HP. The required power is divided evenly among four motors resulting in 0.1417 HP each. This corresponds to a total current draw of 16.18 A, endurance of 12.52 minutes, and corresponding distance of 5.94 miles (31351.2 feet). The speed for best range occurs where the power-velocity curve is tangent to a line from the origin, which is 55.15 ft/s with a corresponding power of 0.6513 HP. Per motor, the required power is 0.1617 HP with a corresponding total current draw of 18.14 A. The resulting flight time and maximum range are 11.16 minutes and 7 miles (36,939 feet), respectively. Selecting a lighter payload will increase the hover endurance, maximum forward-flight endurance, and maximum range from the values listed above. In conclusion, our goal will be to fly the vehicle at the maximum range speed of 55.15 ft/s or 37.6 mph when possible to do so safely.

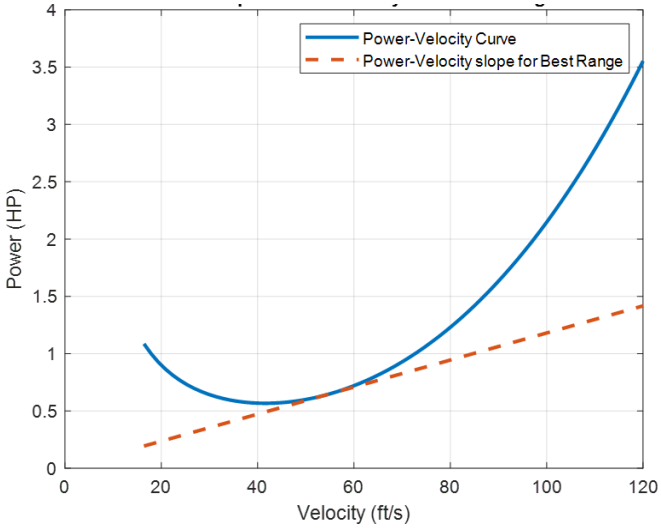

Fig. 12. Power vs Velocity in Forward Flight

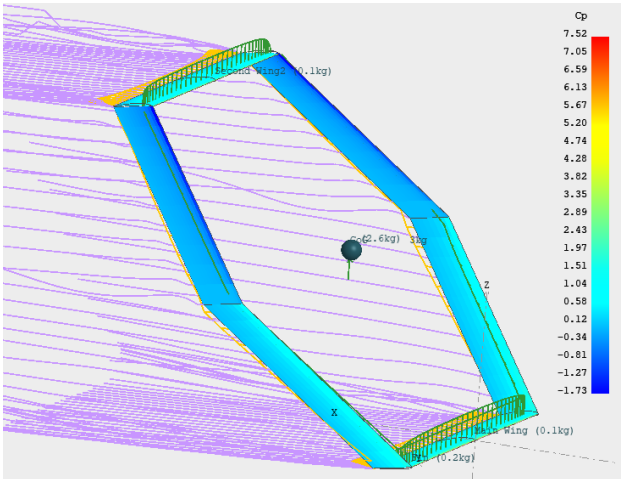

Fig. 13. VLM Analysis of the Aircraft Wings

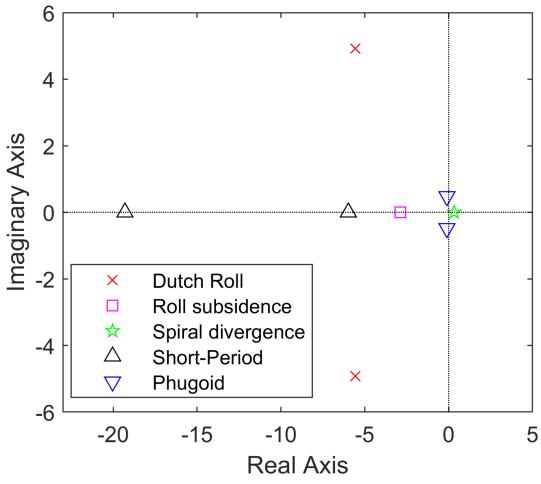

Fig. 14. Longitudinal and Lateral Modes

Aircraft Lift and Drag Estimation: The aircraft wings were modeled in XFLR5 and the Vortex Lattice Method (VLM) was used to calculate the lift and drag distributions. VLM neglects the influence of the thickness and viscosity. In addition to the wings, the fuselage contribution was added based on a 0.5 sq.ft. flat-plate assumption. Since VLM gives the lift and drag coefficients within the stall domain, the linearized model was fused with a globally defined flat-plate model by exponentially weighing their contributions based on the angle of attack. The lift-to-drag ratio of the aircraft in cruise conditions is estimated to be 8. Figure 13 shows the aerodynamic pressure acting on the aircraft's wing along with the lift and drag distribution in cruise mode.

Aircraft Stability Prediction: The rotor effects dominate the aircraft's stability and, hence, in typical flight conditions the control gains are the major factor determining the aircraft's stability. However, if the motor fails, then for safe gliding operation of the aircraft, the wings' stability becomes important. Using the aircraft's wings modeled in XFLR5, longitudinal stability is ensured by placing the aircraft's center of gravity in front of the aerodynamic center. Figure 14 shows the eigenvalues of the longitudinal and lateral modes in the complex plane.

6. Drawing Package

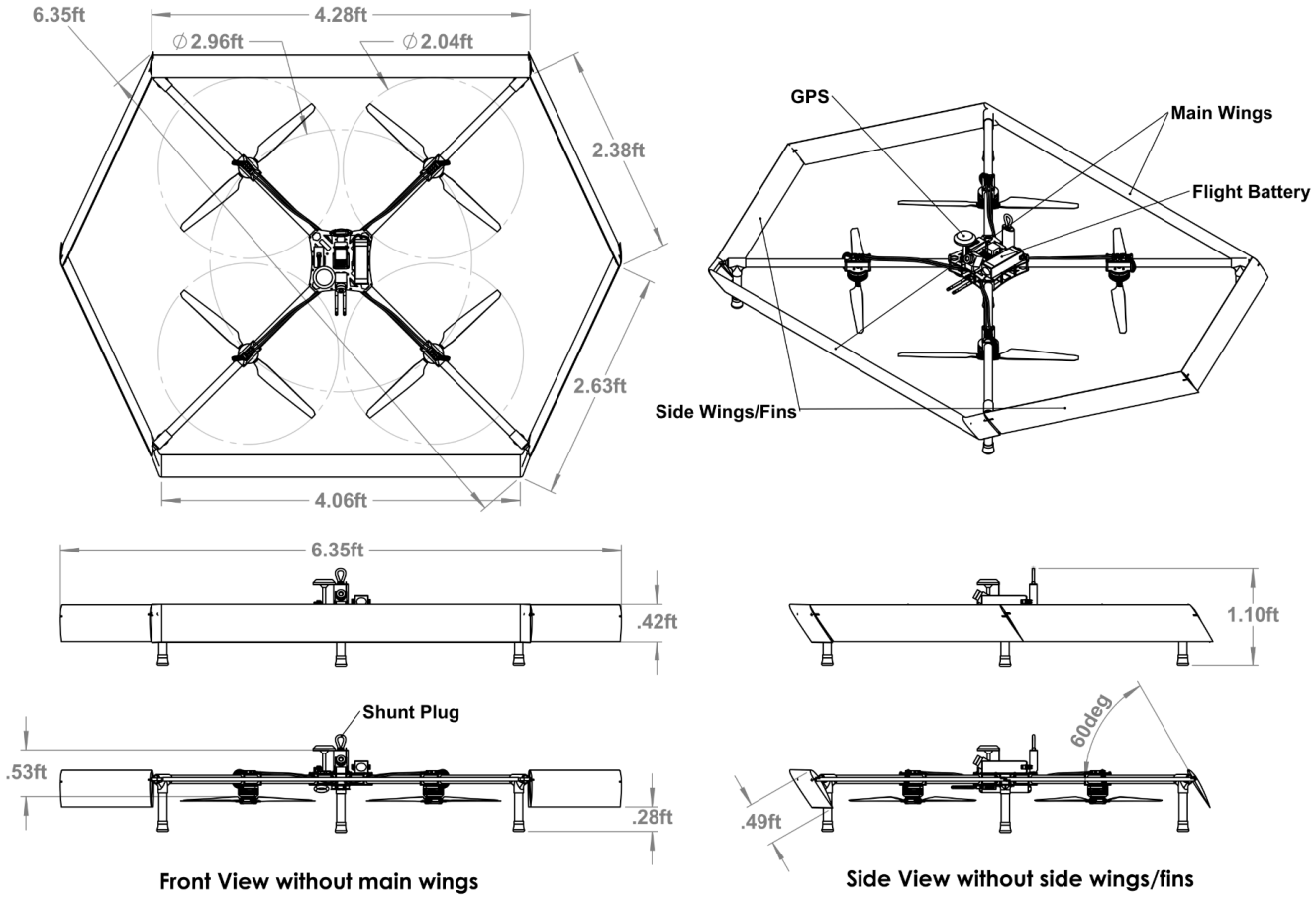

Fig. 15. Three View and Isometric Drawing of the Aircraft

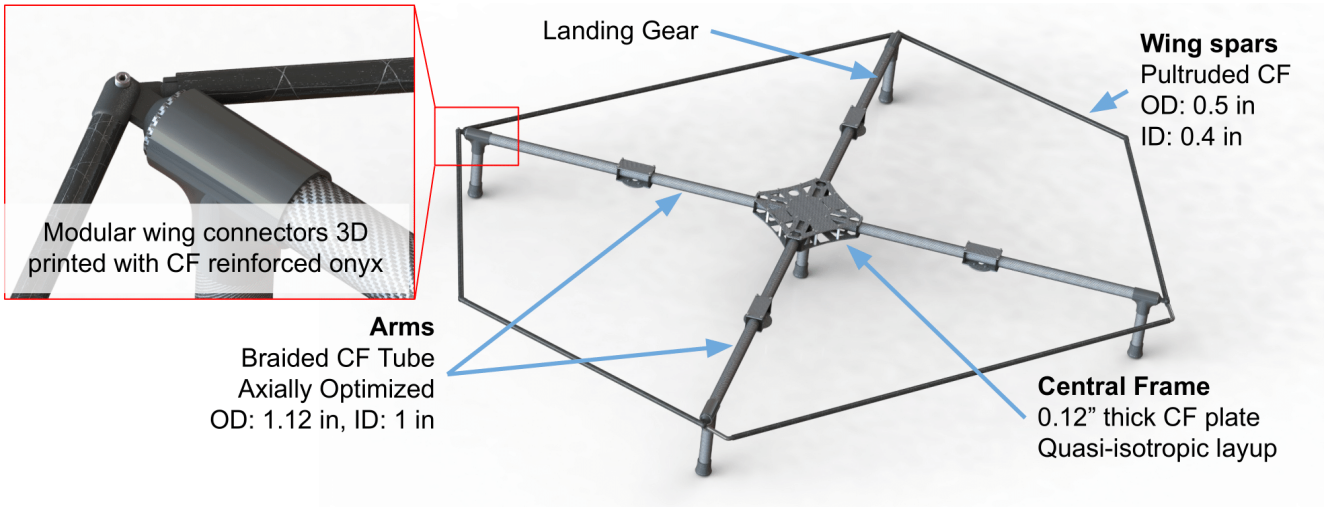

Fig. 16. Arrangement of structural components

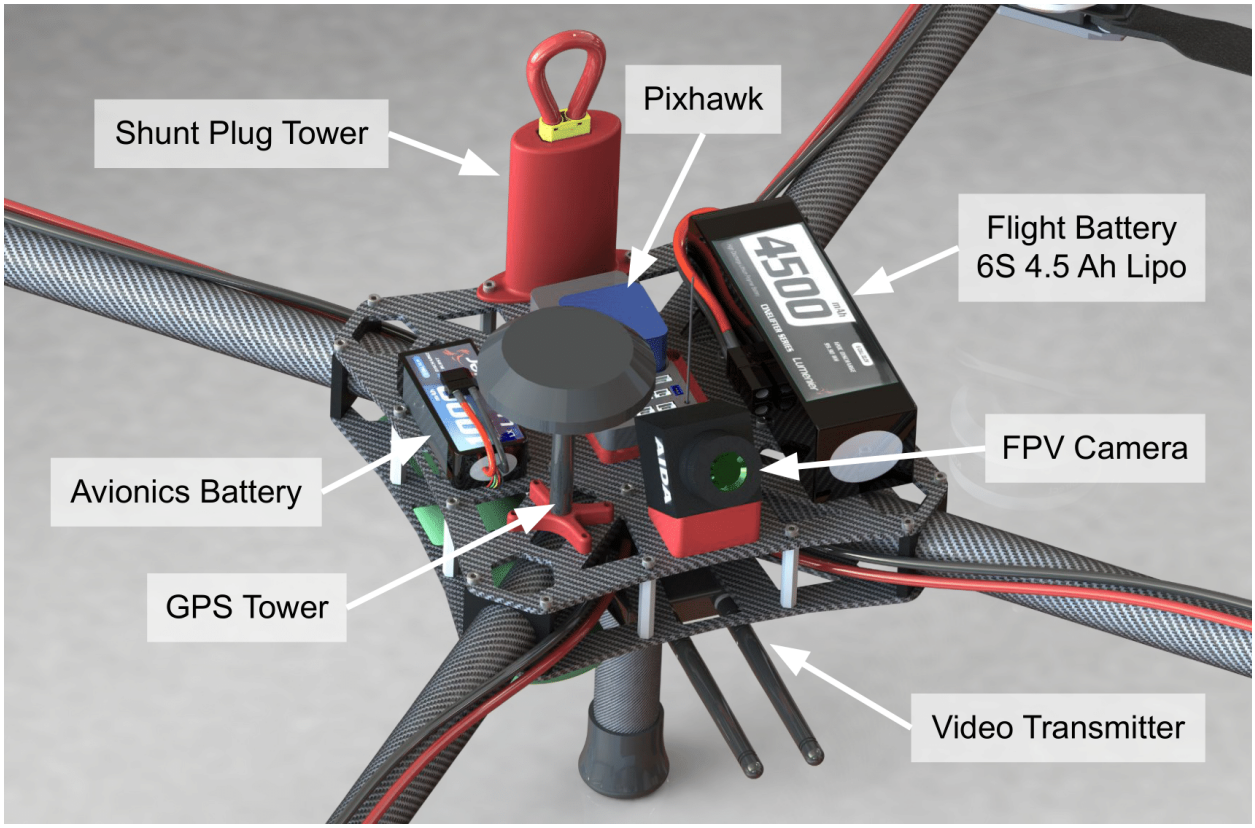

Fig. 17. Layout of Propulsion and Electronics Components on the central frame

7. Fabrication Methods

7.1. Manufacturing processes

Having participated in previous VFS MAV student competitions, the team has experience choosing materials and fabrication methods to be able to quickly manufacture and assemble a completely custom drone in the timeline given by the competition.

7.2. Considered Methods and Materials

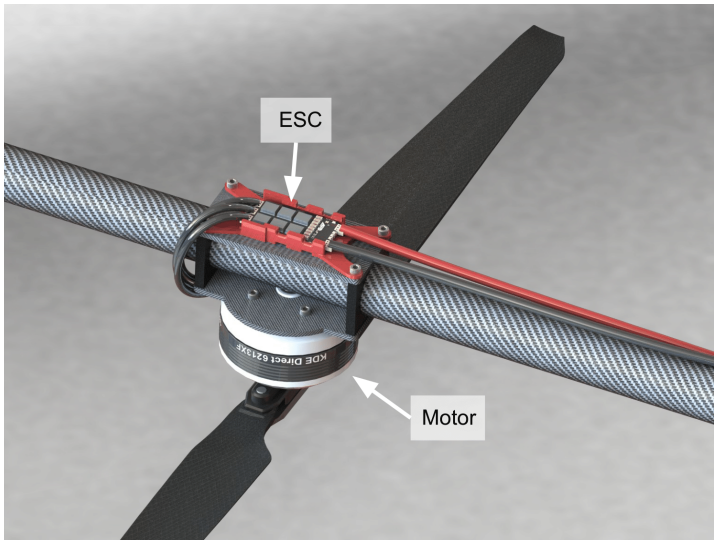

Fig. 18. Layout of Propulsion Components on the arms

CNC Machining: For our main body and structure we considered Dragon Plate, carbon fiber and wood sandwich, and normal carbon fiber. Dragon Plate provides a more lightweight option but it loses strength from using a wood core and has a higher chance of delamination. Due to the complexity of the carbon fiber plate components, we investigated automated machining methods such as CNC and waterjet as the primary means of manufacturing. We observed that waterjet causes delamination and thus we selected CNC machining for cutting the central frame. As for cutting the carbon fiber tubes for arms, CNC would be impractical and expensive and so we manually machined it using dremel tools.

3D Printing: As nearly the entire aircraft is custom made, for structural and non-structural mounting parts, we decided to use 3D printing. The main materials considered were PLA, ABS, HIPS, TPU, Nylon, and Onyx as well as digital materials including Agilus30 black and VeroWhite. Structural components break from bending stresses in a majority of situations and rarely due to tension. Hence, we compared the flexural strength, density, and cost of the different materials in order to select the appropriate materials for structural and non-structural components. The flexural strength for flexible materials such as Agilus30 and TPU are not available and their tensile strength value is more relevant. Table 3 lists the flexural strength, density, and cost of the considered materials. Since Onyx has the highest flexural strength, it was used to print the structural components of the aircraft. Furthermore, its strength can be magnified by orders of magnitude by using Carbon Fiber reinforcement. For non structural components such as the Pixhawk mount, camera mount, ESC mount, etc. we used PLA due to its lower cost while providing sufficient strength. We experimented with flexible materials like TPU and Agilus30 for landing gear components due to their shock absorption properties. Since TPU didn't offer a wider range of material properties we used digital materials to give us a much needed bandwidth of flexibility and stiffness characteristics. Table 2 presents the range of properties that

can be achieved from mixing Agilus30 and Vero. However, these capabilities come at a very high material and printing cost, and therefore they must be used for critical components such as landing gear feet and arm mounting components.

Table 3. Comparison of relevant properties of 3D printing materials

Property	**PLA**	**ABS**	**HIPS**	**Nylon**	**Onyx**	**Vero**	**Agilus30**	**TPU**
Flexural Strength (MPa)	62	37	62	32	81	75	N/A	N/A
Density (g/cm^3)	1.25	1.1	1.08	1.1	1.18	1.17	1.15	1.21
Cost ($/kg)	21	21	39	90	150	300	330	65

7.3. Final Manufacturing Process

Carbon Fiber Components: Carbon-fiber plates and tubes were selected as the primary material for the airframe due to its well known high strength-to-weight property, ease of availability and manufacturability. Carbon-fiber plates with quasi-isotropic inlay and twill weave finish were CNC machined to create the central frame of the aircraft. Off-the-shelf braided and axially optimized carbon fiber tubes were cut to desired lengths to create the arms of the aircraft. Similarly, off the shelf pultruded carbon fiber tubes were cut to desired lengths to create the wing spars. Braided carbon fiber tubes have higher torsional stiffness and thus was ideal for arms. On the contrary, pultruded carbon fiber tubes have unidirectional fibers and thus are ideal for wing spars as they experience mostly bending loads and almost no torsion.

3D printed Components: Onyx reinforced with 9.61cm^3 of Carbon Fiber with isotropic inlay was used to 3D print the wing connectors with the Markforged Mark Two Desktop 3D printer. Using carbon fiber reinforcements, the printed part surpassed our strength requirements, while being able to easily sustain forces from multiple directions due to the Isotropic Fiber inlay pattern. Additionally, it is 22% lighter than the lightest off the shelf available connectors made from aluminum that could interface with our arm and spar design. The landing gear feet and arm mounts were 3D printed using flexible materials to decrease the impulse sustained by the aircraft from frequent takeoff and landing spots in each lap. The landing gear is perpendicular to the ground and must be able to sustain approximately 600N of force loaded axially, 150N per leg. Given this specification, we tested digital materials created by combining Agilus Black photopolymer and Vero White resin. Agilus Black provides tear resistance and flexibility, while Vero White provides rigidity. Different ratios of the two materials were mixed together by the Objet500 Connex3 3D printer to generate materials of varying elasticity and strengths. As explained in Section 4.1, we used FLX9840 for the landing gear feet due to its highest shock absorption from hysteresis and FLX9895 for the landing gear to arm mount in order to balance shock absorption and stiffness.

Assembly: Most of the components on the aircraft were screw-mounted and reinforced with Loctite to diminish the effects of vibration-induced loosening of the screws. Additionally, nuts with nylon inserts were utilized as it grips the bolt to resist loosening without damaging threads. All elements of the aircraft were assembled in the AMAV team's base at the University of

Maryland's Brin Family Aerial Robotics Laboratory. Any components that require soldering or heat shrink tubing were also assembled in the Aerial Robotics Lab soldering stations and subsequently integrated into the aircraft. Acrylic conformal coating was also applied to the exposed PCBs to protect them from dust, light rain, and adverse environmental conditions.

8. Test Plan

Flight tests are planned to be done at UMD Fearless Flight Facility (F3), due to the 15-mile no-fly zone established by the FAA around Washington D.C.. Compared to the 600-foot diameter of Graces Quarters (the competition location), F3 (Figure 19) is 100x300x50 feet, which results in scaled-down tests compared to the competition.

Fig. 19. The UMD Fearless Flight Facility

8.1. Flight Worthiness Test

Test objectives: Determine if the drone is in mechanical, electrical proper condition. Also, determine the FPV video latency is manageable.

Test setup: To examine how well the parts such as motors, propellers, flight controllers are fixed, the drone will be started on the ground and put little thrust to see if the drone tilts to the intended direction and hear the sound of it to examine if the motor operates as intended. To ensure good electrical performance, transmission voltage losses must be within 2% and component's temperatures must be in a safe range during and after flights. The FPV video latency was checked independently in a quantitative manner by measuring it and also qualitatively by flying a smaller drone.

8.2. Hover Endurance Test

Test objectives: Determine how long the drone can hover in place and establish its reliability for the duration of the battery life.

Test setup: The test will be conducted inside the netted area of Fearless Flight Facility (F3) as it is a similar environment with the Graces Quarters test site.

8.3. Cruise Endurance Test

Test objectives: Determine how long the drone can cruise with forward flight.

Test setup: The test will be conducted in F3 autonomously to keep the consistency of the drone's speed. The drone will circle around to make a similar situation of the test. Also the vehicle's extra payload carrying capacity beyond the minimum 2 lb, will be tested.

8.4. Agility and Speed Test

Test objectives: Determine the maneuverability and cornering ability of the drone.

Test setup: In this test, the pilot will manually fly the drone in acrobatic mode (attitude rate control) and push the drone to the limit of its performance.

8.5. Autonomous Flight Test

Test Objectives: Determine how accurate the autonomous capabilities of the drone are by programming numerous waypoints in the testing facility. Additionally, evaluate landing accuracy by characterizing the range of position error using the same autonomous mission and same predetermined landing point to see exactly where the drone lands each time.

Test Setup: The GPS capabilities of the drone is tested by flying in position-hold mode, which is the mainstay prerequisite before testing. Initially, simple waypoint missions like take off, fly 10 feet, and land will be tested. The complexity of these missions is increased to establish reliability, eventually leading up to a mock mission. Furthermore, to test landing accuracy, a simple autonomous mission is created with one landing point and is executed multiple times. After each mission, the landing position of the drone is marked on the ground.

9. Flight Test Results

Flight Worthiness Test [Complete]: The mechanical examination of the aircraft revealed no major issues. The electrical transmission losses measured with a multimeter was within 1% due to the use of 10 awg and 14 awg wires for battery to PDB and PDB to ESC power connections respectively. After flying the aircraft in hover for 10 min indoors, the temperatures of the ESC and Motors were much below their safe operation limits.

Fig. 20. Upgraded FPV Antennas

The FPV system testing on the contrary revealed major issues. The stock antennas of the video transmitters and receivers were linear polarized antennas and had a poor range of 100ft with frequent drops in frame rate beyond 80 ft. Hence, we upgraded the antennas with better off-the-shelf left hand circularly polarized (LHCP) antennas. Circular polarization waves radiate energy not only in horizontal and vertical planes, but also in all planes between them. It also has lower interference losses. We selected lightweight transmitter antennas with cross-polar rejection of -15 to -30 dB and Standing Wave Ratio (SWR) of 1.5:1. For the antennas on the video receiver (Figure 20), we selected antennas with a gain of 10.25 dbic and it featured a patented vector-phasing technology for longer range and better signal clarity. Post antenna upgrade the FPV video latency is around 5 ms and range is around 500 ft.

Hover Endurance Test [Complete]: The hover test was performed indoors without the aircraft wings (Figure 21). In place of the wings, a 1.32 lb payload was added on top of the 2 lb softgrip weight required by the competition. The overall vehicle weight was 14 lb and a hover endurance of 10.5 minutes was achieved. The estimate from the developed rotorcraft power model (Section 4.2) is 10.6 minutes with 15 lb vehicle weight. Possible sources of error are the rectangular untwisted rotor blade shape and uniform inflow assumptions.

Cruise Endurance Test: Not yet completed. See schedule for expected date of completion.

Agility and Speed Test: Not yet completed. See schedule for expected date of completion.

Autonomous Flight Test: Not yet completed. See schedule for expected date of completion.

Fig. 21. Hover test of Foxtail without wings in the Brin Family Aerial Robotics Lab.

10. Conclusion

The technical report describes the entire procedure by which we designed and are in the process of finalizing the building and testing operations of our aircraft for the VFS DBVF competition. We met or exceeded the design requirements and are planning to complete the bonus task as well. The aircraft will be ready before the competition. Ongoing and future work seeks to further enhance the aircraft's performance, decrease its weight, and expand its autonomous capabilities.

11. References

[1] Wayne Johnson, Rotorcraft Aeromechanics, Cambridge University Press, 2013

[2] Traub, Lance. (2011). Range and Endurance Estimates for Battery-Powered Aircraft. Journal of Aircraft. 48. 703-707. 10.2514/1.C031027.